Title
Pacific Influences on Tropical Atlantic Teleconnections to the Southern Hemisphere High Latitudes

Journal
Journal of Climate, 29(18)

ISSN
0894-8755

Authors
Simpkins, Graham R
Peings, Yannick
Magnusdottir, Gudrun

Publication Date
2016-09-15

DOI
10.1175/jcli-d-15-0645.1

Peer reviewed

Pacific Influences on Tropical Atlantic Teleconnections to the Southern Hemisphere High Latitudes

GRAHAM R. SIMPKINS, YANNICK PEINGS, AND GUDRUN MAGNUSDOTTIR

Department of Earth System Science, University of California, Irvine, Irvine, California

(Manuscript received 31 August 2015, in final form 1 June 2016)

ABSTRACT

Several recent studies have connected Antarctic climate variability to tropical Atlantic sea surface temperatures (SST), proposing a Rossby wave response from the Atlantic as the primary dynamical mechanism. In this investigation, reanalysis data and atmospheric general circulation model experiments are used to further diagnose these dynamical links. Focus is placed on the possible mediating role of Pacific processes, motivated by the similar spatial characteristics of Southern Hemisphere (SH) teleconnections associated with tropical Atlantic and Pacific SST variability. During austral winter (JJA), both reanalyses and model simulations reveal that Atlantic teleconnections represent a two-mechanism process, whereby increased tropical Atlantic SST promotes two conditions: 1) an intensification of the local Atlantic Hadley circulation (HC), driven by enhanced interaction between SST anomalies and the ITCZ, that increases convergence at the descending branch, establishing anomalous vorticity forcing from which a Rossby wave emanates, expressed as a pattern of alternating positive and negative geopotential height anomalies across the SH extratropics (the so-called HC-driven components); and 2) perturbations to the zonal Walker circulation (WC), driven primarily by an SST-induced amplification, that creates a pattern of anomalous upper-level convergence across the central/western Pacific, from which an ENSO-like Rossby wave train can be triggered (the so-called WC-driven components). While the former are found to dominate, the WC-driven components play a subsidiary yet important role. Indeed, it is the superposition of these two separate but interrelated mechanisms that gives the overall observed response. By demonstrating an additional Pacific-related component to Atlantic teleconnections, this study highlights the need to consider Atlantic–Pacific interactions when diagnosing tropical-related climate variability in the SH extratropics.

1. Introduction

In recent decades, considerable regional-scale climatic changes have been observed at the Southern Hemisphere (SH) high latitudes (Turner et al. 2005). These are perhaps most clearly illustrated by the rapid warming of the Antarctic Peninsula and continental West Antarctica (Vaughan et al. 2003; Bromwich et al. 2013), as well as the pronounced dipole-like redistribution of sea ice, characterized by increases in the Ross Sea and decreases in the Amundsen–Bellingshausen Seas (Parkinson and Cavalieri 2012; Simpkins et al. 2013). The spatial asymmetry of these changes alludes to strong connections with the large-scale atmospheric circulation, specifically to perturbations in the Amundsen Sea low (ASL), a semipermanent region of low pressure in the South Pacific sector of the Southern Ocean (e.g., Turner et al. 2013; Raphael et al. 2016). The ASL is a key component of the nonzonal circulation, controlling meridional winds over much of West Antarctica, and thus exerting a pronounced impact on its climate (e.g., Hosking et al. 2013). Wind-driven changes in ice advection, for example, have been suggested as the dominant cause of sea ice trends around much of West Antarctica (Holland and Kwok 2012), consistent with the observed deepening of the ASL (Turner et al. 2009).

Several studies have shown that the position and intensity of the ASL is influenced by patterns of large-scale climate variability, namely the southern annular mode (SAM) and the high-latitude response to El Niño–Southern Oscillation (ENSO). The SAM is the leading mode of climate variability in the SH and describes a seesaw in atmospheric pressure anomalies between the

Corresponding author address: Graham R Simpkins, Dept. of Earth System Science, University of California, Irvine, 3200 Croul Hall, Irvine, CA 92697.
E-mail: g.simpkins@uci.edu

DOI: 10.1175/JCLI-D-15-0645.1

middle and high southern latitudes (Thompson and Wallace 2000). Although annular by definition, the SAM possesses a significant nonannular component, expressed as locally enhanced pressure anomalies over the ASL region (Simpkins et al. 2012). Numerous studies have also connected the Antarctic circulation to Pacific sea surface temperature (SST) (e.g., Karoly 1989; Turner 2004; Simpkins et al. 2012; Ciasto et al. 2015). Driven by tropical heating and associated deep convection during El Niño events, upper-level vorticity anomalies excite a pattern of stationary Rossby waves that propagate to the SH high latitudes in a great arc (Hoskins and Karoly 1981; Rasmusson and Mo 1993; Trenberth et al. 1998). The resulting wave train manifests as cyclonic anomalies off western New Zealand, anticyclonic anomalies over the ASL, and cyclonic anomalies off South America. This atmospheric signature has been termed the Pacific–South American (PSA) teleconnection pattern (Mo 2000); it exhibits seasonal variability in its spatial structure (Simpkins et al. 2012) and further highlights the importance of nonannular atmospheric variability in the SH climate (Matthewman and Magnusdottir 2012). During austral winter and spring, Pacific SST trends have also been connected to the observed deepening of the ASL and the associated regional surface air temperature (SAT) and sea ice trends (Ding et al. 2011; Schneider et al. 2012; Clem and Fogt 2015).

More recently, tropical Atlantic SST variability has been related to circulation anomalies around Antarctica (Okumura et al. 2012; Li et al. 2014, 2015a,b; Simpkins et al. 2014). Driven by Atlantic warming, these teleconnections are associated with an intensification of the local Hadley cell, and the resulting development of Rossby waves at the descending branch by upper-level vorticity anomalies (Simpkins et al. 2014). In both observations and models, the wave train promotes a significant deepening of the ASL in all seasons except austral summer, highlighting a seasonality to the teleconnection that is governed by the strength and extension of the subtropical jet (Li et al. 2015a). While geopotential height anomalies associated with Atlantic teleconnections are largely centered over the ASL, significant features are also observed over the subtropical Pacific (e.g., Li et al. 2015a, their Fig. 2). As such, Atlantic teleconnections bear (partial) resemblance to the high-latitude response to ENSO, suggesting a potential mediating influence of the Pacific, as proposed by both Li et al. (2014, 2015a) and Simpkins et al. (2014). This possible interaction has not previously been examined in relation to extratropical teleconnections, and thereby becomes the focus of this investigation.

Several studies, however, have determined the relationships between equatorial Atlantic and Pacific SST. Atlantic Niño, also referred to as the equatorial or zonal mode, is the leading pattern of tropical Atlantic SST variability. It is similar to its Pacific counterpart, but differs in that SST anomalies are weaker, events are of shorter duration, and peaks occur during austral winter (Zebiak 1993; Xie and Carton 2004; Keenlyside and Latif 2007). A time-delayed impact of Atlantic Niño on ENSO has been well established in both observations and models, wherein Atlantic SST anomalies tend to precede those in the Pacific by ~6 months (Keenlyside and Latif 2007). Indeed, partially coupled model experiments, forced with observed SST anomalies in the Atlantic but a fully coupled Pacific, favor the development of a La Niña–like SST pattern (Ding et al. 2012). This connection can be explained through modifications to the Walker circulation (WC), the atmospheric bridge between the basins: during an Atlantic Niño event, a strengthened WC drives westward surface wind anomalies over the Pacific, increasing the east–west thermocline gradient, and encouraging negative SST anomalies that are subsequently amplified through Bjerknes feedback (Rodríguez-Fonseca et al. 2009; Losada et al. 2010; Ding et al. 2012). An enhanced interbasin SST gradient between the Atlantic and Pacific will also act to strengthen WC signals (Wang 2006).

While causal links have been established from the perspective of Atlantic SST variability influencing the Pacific (e.g., Ding et al. 2012), the converse is also true, complicating the interpretation of interbasin interactions. El Niño events, for example, are known to mediate anomalous warming in the northern tropical Atlantic through a corresponding weakening of the trade winds (Enfield and Mayer 1997; Sutton et al. 2000; Alexander et al. 2002; Chang et al. 2006). The connection with the southern equatorial Atlantic (i.e., the Atlantic Niño domain), however, is far less clear, with El Niño events sometimes followed by warm anomalies, and other times by cold (Huang 2004; Chang et al. 2006; Lübbecke and McPhaden 2012). This inconsistency has been interpreted in terms of competing dynamical and thermodynamical processes (Chang et al. 2006) and a delayed negative SST feedback (Lübbecke and McPhaden 2012). Regardless of the cause, this lack of a clear relationship hints at a more dominant direction of causality from Atlantic to Pacific, especially for the southern equatorial Atlantic and at the shorter time scales investigated here. Nevertheless, it is important to recognize that interbasin interactions do not occur unidirectionally, complicating the diagnosis of SH tropical teleconnections.

Given the established relationships between Atlantic and Pacific SST variability, and that the high-latitude SH teleconnection signatures from both basins exhibit similar spatial characteristics, this study aims to determine

whether Pacific signals confound the interpretation of Atlantic teleconnections. Using a suite of observational datasets and atmospheric general circulation model (AGCM) experiments, we specifically address the following questions: 1) To what extent, if any, do Pacific processes mediate Atlantic teleconnections? and 2) What are the physical mechanisms driving these interactions and subsequent teleconnections? In doing so we build upon previous literature which examines the impacts and dynamics of Atlantic teleconnections (Li et al. 2014, 2015a,b; Simpkins et al. 2014), thus furthering our understanding of how tropical fluctuations may be linked to high-latitude climate variability and change (e.g., Ding et al. 2011; Schneider et al. 2012; Li et al. 2014; Clem and Fogt 2015).

The paper is structured as follows: datasets, methods, and numerical simulations are described in section 2, followed by an observational analysis of Atlantic–Pacific interactions in section 3a. Given distinct synchronous variability between tropical Atlantic SST and the Pacific atmosphere during austral winter (June–August), the resulting teleconnections from both basins are compared in section 3b, demonstrating that Atlantic teleconnections may reflect both Atlantic and Pacific-driven components. The dynamics of such teleconnections are subsequently explored using observations (section 3c) and AGCM experiments (sections 3d and 3e). A two-mechanism process is proposed, wherein tropical Atlantic SST variability drives two occurrences: 1) an intensification of the local Atlantic Hadley circulation (HC), establishing an anomalous vorticity source at the descending branch, and triggering a wave train which is characterized by an alternating pattern of positive and negative height anomalies in the SH extratropics; and 2) a perturbation to the zonal Walker circulation, driven largely through Pacific SST-induced amplification, which results in upper-level vorticity anomalies over the central Pacific, exciting a Rossby wave train that extends to West Antarctica. The superposition of these two components is believed to give the total teleconnection pattern we observe. A summary and discussion are provided in section 4.

2. Data, methods, and numerical simulations

a. Observational and reanalysis datasets

Its study, interactions between the tropical Atlantic and Pacific, as well as the subsequent teleconnections to the SH high latitudes, are initially examined using various observational datasets. Monthly-mean SST are from the Hadley Centre Global Sea Ice and Sea Surface Temperature dataset (HadISST; Rayner et al. 2003). Atmospheric fields, including 200-hPa geopotential height (Z_{200}), 200-hPa divergence, sea level pressure (SLP), zonal (U) and meridional (V) winds, and vertical velocity (W) are from the ERA-Interim reanalysis (Dee et al. 2011). ERA-Interim was used over alternative reanalysis products because of its better performance at the SH high latitudes (e.g., Bracegirdle 2013); we note, however, that repeating analyses with different datasets (e.g., NCEP and MERRA reanalyses) yields quantitatively similar results to those presented here (see also Li et al. 2015a). Precipitation is taken from the CPC Merged Analysis of Precipitation (CMAP; Xie and Arkin 1997). All observational products are constrained to the post-satellite period, 1979–2014, to maximize spatial and temporal data coverage in the SH high latitudes.

b. Indices

Tropical SST variability in the Atlantic and Pacific is described by the Atlantic-3 (ATL3) and Niño-3.4 (N3.4) SST indices, respectively. The ATL3 index is defined as area-averaged SST anomalies over 3°N–3°S, 0°–20°E: positive (negative) values refer to warm or Atlantic Niño (cold or Atlantic Niña) conditions. While generic indices of tropical Atlantic SST (e.g., anomalies averaged over 20°N–20°S; Li et al. 2014, 2015a) are significantly correlated with ATL3 (0.78 based on all months), analyses are focused on the latter in order to encapsulate more realistic SST variability and quantify the southern high-latitude impacts of this leading tropical Atlantic mode (Keenlyside and Latif 2007). The N3.4 index is defined as area-averaged SST anomalies over 5°N–5°S, 120°–170°W, wherein positive values reflect warm or El Niño conditions. The spatial domains encompassed by ATL3 and N3.4 indices are shown as black boxes in Fig. 1a.

To additionally gauge the response of the Pacific atmosphere to ATL3 events, we quantify the equatorial Southern Oscillation index (eqSOI). The eqSOI is defined as the difference of standardized SLP anomalies between the east Pacific (5°N/S, 80°–130°W) and Indonesian (5°N/S, 90°–140°E) regions. It is highly correlated with the traditional Southern Oscillation index (SOI; 0.76 based on all months) but is used to capture more of the large-scale WC variability. Prior to analysis, all indices are standardized such that subsequent regressions relate to a one standard deviation positive event.

c. Data processing and statistical methods

Monthly anomalies for all datasets are computed by subtracting the long-term climatological monthly mean. These are subsequently converted to seasonal mean anomalies by averaging over austral summer [December–February (DJF)], fall [March–May (MAM)], winter [June–August (JJA)] and spring [September–November (SON)]

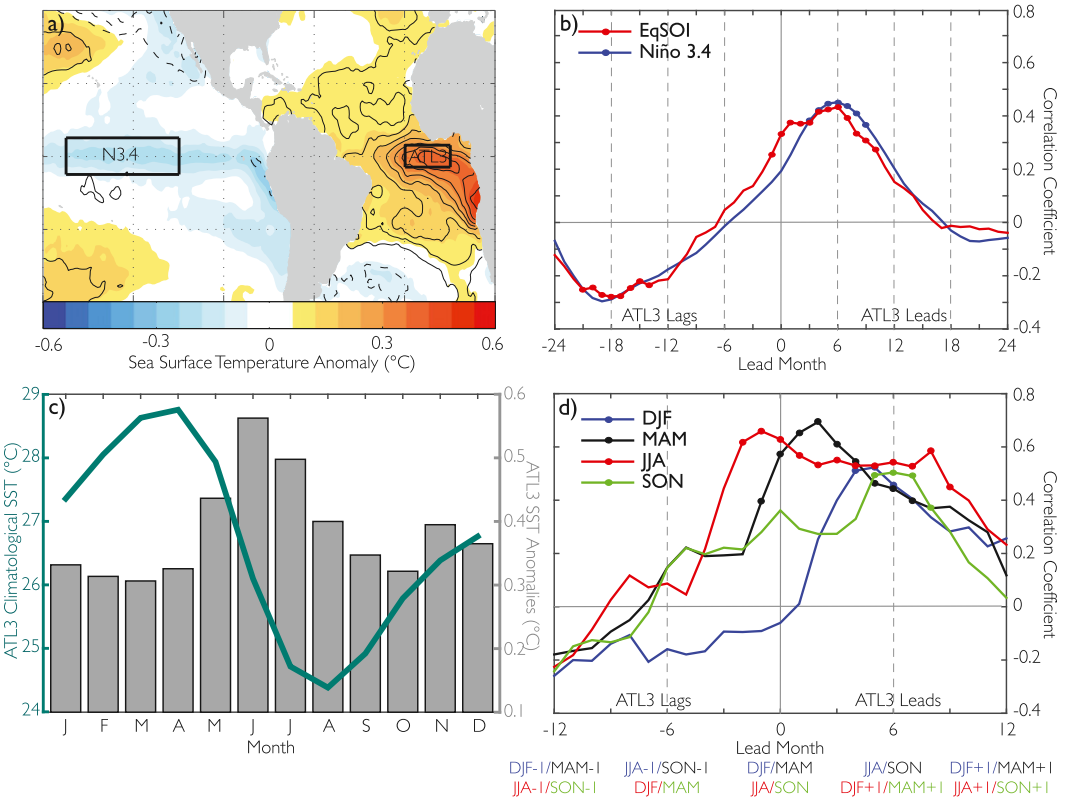

FIG. 1. (a) Monthly-mean SST anomalies regressed onto the standardized ATL3 index (shading), and ATL3 index with Niño-3.4 linearly removed (contours), for all months. Solid (dashed) contours denote positive (negative) anomalies, and are drawn at 0.05°C increments. Black boxes outline the regions used to define the Niño-3.4 (N3.4) and Atlantic-3 (ATL3) SST indices. (b) Lead–lag correlations of the ATL3 index with the N3.4 (blue) and equatorial SOI (eqSOI; red) indices; N3.4 indices have been inverted. (c) Monthly climatological SST (green line) and SST anomalies associated with Atlantic Niño events (gray bars) averaged across the ATL3 domain. (d) Seasonal lead–lag correlations between the ATL3 and eqSOI indices for DJF (blue), MAM (black), JJA (red), and SON (green). In (b) and (d), circle markers highlight correlations significant at the 95% confidence level according to a two-tailed Student's *t* test. Positive leads illustrate ATL3 leading the eqSOI.

and detrended by removing the linear trend. The primary statistical tools that make use of these monthly and seasonal mean anomalies are regression and correlation analysis. The statistical significance of correlation and regression coefficients is measured using the *t* statistic, wherein the effective sample size is estimated based on the lag-1 autocorrelation of the two time series (Bretherton et al. 1999). A 95% threshold of significance is used for all analyses.

d. Model setup and experimental design

To validate observational results and further constrain the dynamics of Atlantic teleconnections, numerical experiments are performed using the NCAR Community Atmosphere Model, version 5 (CAM5; Neale et al. 2012). For all simulations, CAM5 is configured at approximately 1.9° × 2.5° latitude/longitude resolution with 30 vertical levels. Greenhouse gas, ozone, and aerosol concentrations are held constant at values representative of the year 2000.

The control (CTL) experiment is an 80-yr-long simulation in which CAM5 is forced with a monthly repeating cycle of climatological SST and sea ice concentration from the HadISST dataset over 1980–2007. Two further primary idealized experiments are performed in which only the SST boundary conditions are modified:

1) *ATL3W*, to assess the impact of positive (or warm) ATL3 events. For this experiment the pattern of monthly SST anomalies associated with ATL3, as determined through monthly regressions, is superimposed on the background climatology (see Fig. A1 for SST forcing). To avoid unrelated atmospheric responses beyond the regions of interest, the superimposed SST anomalies were constrained to the Atlantic and Pacific Oceans between 15°N and 25°S. Linear damping was applied at these boundaries

over a 5° latitude band to further minimize spurious signals. While SST anomalies are observed in the Indian Ocean, these are of comparatively minor amplitude, and are thus excluded from the perturbation experiments for simplification.

2) *ATL3C*, to assess the impact of negative (or cold) ATL3 events. This experiment was performed as above, but with the superimposed SST anomalies inverted to represent a linearly opposing negative event.

While particular emphasis is placed on the ATL3W/ATL3C experiments, representing the full idealized response to ATL3 SST variability, we additionally perform a complementary suite of numerical simulations in which the superimposed ATL3-related SST anomalies are individually constrained to the tropical Atlantic and Pacific. These experiments were run for both the warm and cold cases, and are subscripted with AO for "Atlantic only" ($ATL3W_{AO}$/$ATL3C_{AO}$) and PO for "Pacific only" ($ATL3W_{PO}$/$ATL3C_{PO}$). Such simulations verify the dominant role of Atlantic SST anomalies and further allow us to elucidate the possible feedbacks associated with Atlantic–Pacific interactions.

As in the CTL, both ATL3W and ATL3C (as well as their Atlantic- and Pacific-only counterparts) were run for 80 years, providing 80 individual members with constant SST forcing. For all simulations, one year of spinup is completed prior to analysis. The atmospheric response to the Atlantic forcing is determined by subtracting the corresponding CTL and analyzing the 80-yr mean. In what follows, model results are subsequently presented as the difference between the warm and cold simulations, that is ATL3W − ATL3C, $ATL3W_{AO}$ − $ATL3C_{AO}$, and $ATL3W_{PO}$ − $ATL3C_{PO}$.

3. Results

a. *Observational evidence of tropical Atlantic–Pacific interactions*

Given established linkages between tropical Atlantic and Pacific SST variability (e.g., Keenlyside and Latif 2007; Rodríguez-Fonseca et al. 2009; Ding et al. 2012), and that both exhibit connections to the SH atmospheric circulation with similar spatial characteristics (e.g., Karoly 1989; Simpkins et al. 2012, 2014; Li et al. 2014, 2015a), it is prudent to revisit these interactions to determine whether they have any bearing on subsequent Atlantic teleconnections.

Figure 1a shows the contemporaneous spatial pattern of SST anomalies associated with the monthly-derived ATL3 index. While peak SST anomalies are located in the Gulf of Guinea, simultaneous variability is observed throughout the tropical Pacific, representative of a weak La Niña pattern. Accordingly, a zero-lag correlation of −0.20 is observed between the ATL3 and N3.4 SST indices (Fig. 1b, blue line; note that N3.4 values have been inverted), although this lacks statistical significance. Peak correlations are observed when ATL3 leads N3.4 by ~6 months (Fig. 1b), which, consistent with previous modeling studies (Rodríguez-Fonseca et al. 2009; Ding et al. 2012; Kucharski et al. 2015), represents the time-delayed impact of Bjerknes feedback and associated mechanisms. No significant relationship is observed when N3.4 leads ATL3 (Enfield and Mayer 1997; Chang et al. 2006; Ding et al. 2012). Associations with the eqSOI (which characterizes the state of the Pacific atmosphere) exhibit similar characteristics to N3.4 (Fig. 1b, red line), but a significant synchronous correlation of 0.34 is observed. These results suggest the Pacific atmosphere may respond more quickly to ATL3 variability than the underlying SST (Fig. 1b; cf. blue and red lines). While these statistical relationships cannot address causality, the pronounced skew toward Atlantic leading is indicative of a more dominant direction of impact from Atlantic to Pacific, reinforcing the conclusions of previous model-based investigations (e.g., Chang et al. 2006; Ding et al. 2012; Lübbecke and McPhaden 2012). As significant zero-lag correlations are only found for the eqSOI, this subsequently becomes the primary index used to represent Pacific variability.

While Fig. 1b demonstrates significant contemporaneous relationships to the eqSOI over all months, Atlantic Niño events exhibit a pronounced annual cycle that may promote seasonality to Atlantic–Pacific interactions. Specifically, SST variability in the ATL3 region is heightened in late fall/early winter, reaching a peak amplitude of 0.55°C in June (Fig. 1c; see also Zebiak 1993; Keenlyside and Latif 2007). Seasonal correlations between ATL3 and the eqSOI reflect a similar pattern, attaining a zero-lag maximum for JJA (0.64; Fig. 1d, red line), when SST anomalies are strongest, and a minimum for DJF (−0.05; Fig. 1d, blue line) when SST anomalies are weakest. Significant wintertime correlations when ATL3 lags by 1–2 months are largely believed to result from the inclusion of pronounced June SST anomalies. Figure 1d also reveals that ATL3 generally leads the eqSOI on seasonal time scales, further suggesting that Atlantic influences on the Pacific likely dominate, particularly near zero-lag during MAM and JJA (see also Ding et al. 2012). Given the well-established connections between atmospheric disturbances in the tropical Pacific and the excitation of atmospheric Rossby waves (Karoly 1989), and that ~40% of eqSOI variability can seemingly be linked to ATL3 in JJA (i.e., given $r = 0.64$, and assuming an association from Atlantic to Pacific), observed Atlantic

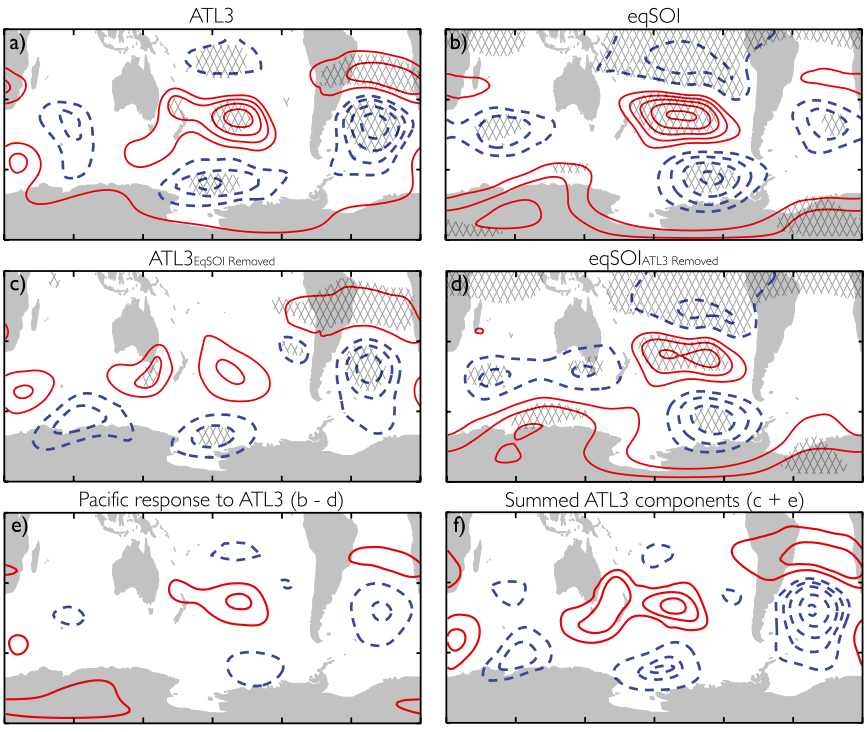

FIG. 2. JJA Z_{200} anomalies regressed onto the (a) JJA ATL3 index, (b) JJA eqSOI index, (c) JJA ATL3 with eqSOI removed through linear regression, and (d) JJA eqSOI index with ATL3 removed through linear regression. (e) The estimated Pacific response to ATL3, that is (b)–(d). (f) The sum of the Atlantic and Pacific components, that is (c) + (e). Solid red (dashed blue) contours represent positive (negative) anomalies, and are drawn at 4-m intervals. Hatching highlights significance at the 95% confidence level.

teleconnections may inherently possess Pacific signals. Motivated by this peak wintertime interaction, subsequent analyses of high-latitude teleconnections focus explicitly on JJA, which also coincides with the season during which heightened tropical–extratropical interactions occur (Jin and Kirtman 2009; Simpkins et al. 2012), and when background climatological conditions allow Atlantic teleconnections (Li et al. 2015a).

Given the focus on SH high-latitude teleconnections, it is necessary to also briefly assess any possible relationships between ATL3 and the leading mode of SH climate variability, the SAM. During JJA, the ATL3 and SAM indices (the latter expressed as the leading principal component of 500-mb heights) are uncorrelated at 0.01; similarly, no significant relationship is observed with N3.4 or the eqSOI. As such, any subsequent teleconnections, as outlined in section 3b, are independent of the SAM.

b. *Comparison of observed Atlantic and Pacific teleconnections*

As alluded to in Fig. 1, the interpretation and understanding of Atlantic teleconnections may be confounded by interactions with the Pacific. Figures 2a and 2b thus compare the high-latitude atmospheric signatures of ATL3 and the eqSOI, respectively, by regressing JJA Z_{200} anomalies onto the corresponding detrended standardized index; solid red (dashed blue) contours denote positive (negative) height anomalies, and hatching highlights regressions significant at the 95% level according to two-tailed Student's t tests. While results are presented only for Z_{200}, the corresponding teleconnections are found to exhibit an equivalent barotropic structure (not shown).

The high-latitude teleconnections for ATL3 (Fig. 2a) and the eqSOI (Fig. 2b) project very strongly onto one another, exhibiting a spatial correlation of 0.74. In both cases, significant geopotential height anomalies are observed over the Atlantic and Pacific Oceans, but with enhanced magnitudes in the respective basin. Atlantic anomalies are characterized by contrasting pressure centers between the subtropics and midlatitudes, while Pacific anomalies represent the high-latitude response to ENSO; a wave train that appears as positive pressure anomalies over the subtropical Pacific, negative pressure anomalies over the ASL, and positive pressure anomalies over Antarctica, resembling the seasonal teleconnections

observed in several studies (e.g., Simpkins et al. 2012; Ciasto et al. 2015). This Pacific-centered pattern shall be termed "ENSO-like." Although the large-scale spatial structures are highly consistent, differences are apparent in the location and magnitude of pressure centers. For example, the negative geopotential heights observed over the high-latitude South Pacific are strengthened and shifted eastward toward the Antarctic Peninsula when comparing eqSOI teleconnections to ATL3. The ATL3-related pattern is found to be highly consistent in both structure and magnitude with that of Li et al. (2015a), who performed regressions using an index of tropical Atlantic SST (see their Fig. 2).

The pronounced similarities described above indicate that some component of Atlantic teleconnections, specifically the ENSO-like Z_{200} anomalies, may be driven by Pacific processes associated with Atlantic–Pacific interactions (Fig. 1). To further examine this possibility, analyses are repeated using indices in which the eqSOI has been removed from ATL3 using linear regression ($ATL3_{eqSOIRemoved}$), and where ATL3 has been removed from the eqSOI ($eqSOI_{ATL3Removed}$) using the same technique.

When isolating the impact of Atlantic SST variability (Fig. 2c), the corresponding teleconnection takes a markedly different form (cf. Figs. 2a and 2c). The dominant ENSO-like pattern has been replaced with a wavelike structure emanating from the subtropical Atlantic, exhibiting an alternating pattern of positive and negative height anomalies spanning the SH high latitudes. Several of these significant wave train features are collocated with, or near, centers of the ENSO-like pattern, including the negative heights observed over the Ross Sea. These wavelike features are also found in composite analyses of positive ATL3/neutral eqSOI events (not shown) and are consistent with the Rossby wave train hypothesis presented in Simpkins et al. (2014) and Li et al. (2015a,b). When the impact of ATL3 is removed from the eqSOI (Fig. 2d), however, the large-scale teleconnection structure remains mostly unchanged, except the distinct loss of Atlantic signals coupled with reduced magnitude anomalies (cf. Figs. 2b and 2d). The difference between regression patterns associated with eqSOI (Fig. 2b) and $eqSOI_{ATL3Removed}$ (Fig. 2d), as illustrated in Fig. 2e, thereby provides an estimation of the ATL3-related Pacific teleconnection response, and reveals weakened ENSO-like features.

Examining these teleconnections in isolation reveals that Atlantic impacts on the SH high latitudes (Fig. 2a) may result from two simultaneous and interacting processes: 1) the wavelike anomalies driven directly by Atlantic SST variability (Fig. 2c) and 2) the weakened ENSO-like features triggered in the Pacific (Fig. 2e) and driven through Atlantic–Pacific interactions (Fig. 1d). It is the superposition of these structures, which share many overlapping centers of action, that gives the total teleconnection observed in Fig. 2a. Indeed, when summing Figs. 2c and 2e (i.e., an estimation of the Atlantic and Pacific responses, respectively), the result strongly resembles the original ATL3 teleconnection, exhibiting a spatial correlation of 0.85 (cf. Figs. 2a and 2f), and adding credence to the two-mechanism hypothesis; the subtle differences may arise from nonlinear interactions, the possible weak impact of Indian Ocean SST anomalies, or the subsequent amplification following SST feedbacks in the Pacific. In the following section we examine the atmospheric dynamics behind these processes. Before doing so, however, it is important to note that ATL3 teleconnections explain only a small component of ASL variability (maximum 15 m), emphasizing the dominant role of alternative processes in driving changes in this highly variable region.

c. *Dynamical mechanisms of Atlantic teleconnections*

Following the discussion above, the tropical dynamics that promote the hypothesized two-mechanism Atlantic teleconnections are evaluated using observational and reanalysis data. Figure 3 illustrates simultaneous wintertime regressions of various tropical anomalies with the ATL3 index; recall that indices are standardized such that all panels show results for a one standard deviation positive event. We begin by diagnosing the Pacific-centered Z_{200} anomalies (i.e., the triggering of the ENSO-like signals) believed to be associated with Atlantic–Pacific interactions (Fig. 2e).

Driven by the positive ATL3-related SST forcing (Fig. 3a, shading), the tropical system undergoes a series of changes that can broadly be categorized into a direct and indirect Pacific response, consistent with the mechanisms outlined in Li et al. (2015c). The direct response is reminiscent of Gill's solution to tropical heating. Anomalous deep convection over the equatorial Atlantic, characterized by ascending motion (Fig. 3b, blue shading) and increased precipitation (Fig. 3a, green contours), drives westerly (easterly) wind anomalies over the eastern (Indo/western) Pacific in the form of Rossby (Kelvin) waves (Fig. 3a, vectors; Fig. 3b, contours). As a result of wind–evaporation–SST feedbacks, these anomalous wind conditions consequently promote cooling in the east and warming in the west, encouraging a La Niña–like SST pattern (Fig. 3a, shading). In addition, westward wind anomalies over much of the Indo/western Pacific enhance the thermocline through shoaling in the east and deepening in the west, further encouraging anomalous SST conditions, especially in the central Pacific. Such atmospheric conditions can similarly be expressed as perturbations to

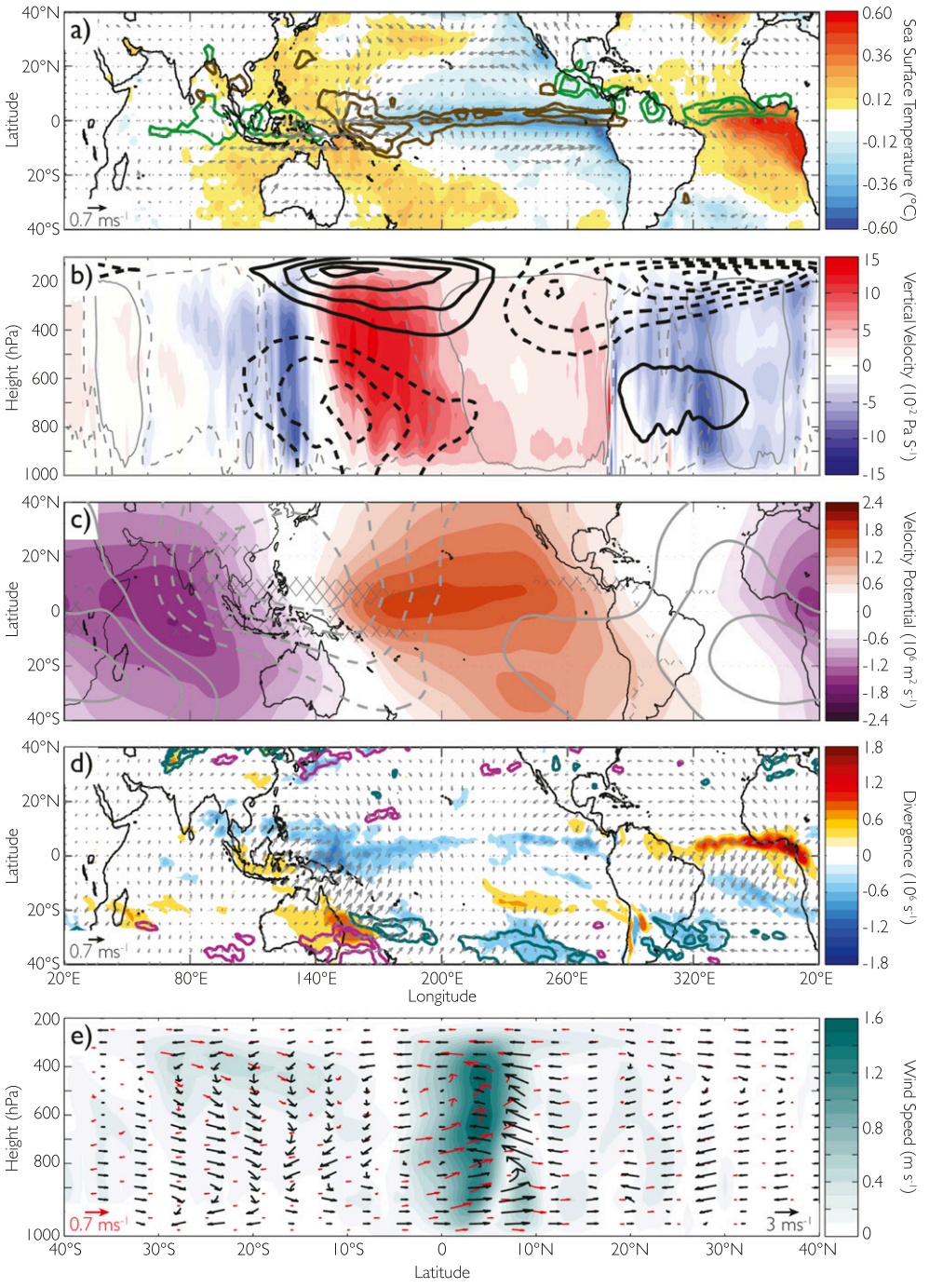

FIG. 3. (a) JJA SST (shading), 925-hPa winds (vectors), and precipitation (contours); (b) vertical velocity (shading) and zonal wind (contours) averaged over 5°N/S; (c) 200-hPa velocity potential (shading); (d) 200-hPa divergence (shading), divergent winds (vectors), and Rossby wave source (contours); and (e) Atlantic Hadley circulation wind speed (shading) and winds (red vectors), regressed onto JJA ATL3 index. In (a), green (brown) contours denote increased (decreased) precipitation, drawn at 0.5 mm day^{-1} intervals. In (b) solid (dashed) contours denote positive/eastward (negative/westward) winds, drawn at 0.5 m s^{-1} intervals. Gray contours mark the climatological vertical velocity averaged over 5°N/S, with solid (dashed) contours indicating the boundaries of descending (ascending) cells at 0.01 m s^{-1}. In (c), contours represent the climatological mean velocity potential, with solid (dashed) contours denoting negative (positive) values drawn at 4×10^6 m^2 s^{-1}, and hatching where climatological ascending motion is observed. In (d), pink (turquoise) contours denote positive (negative) Rossby wave source anomalies, drawn at 0.25×10^{-6} s^{-2} intervals. In (e), vectors are quantified using vertical velocity and the V component of divergent winds, with black denoting the climatological mean calculated over 1979–2014. Shading corresponds to wind speed, also calculated using vertical velocity and V divergent winds.

the zonal Walker circulation (Fig. 3b). Latent heat release over the equatorial Atlantic promotes a pattern of negative velocity potential (Fig. 3c, purple shading) or upper-level divergence (Fig. 3d, red shading), which, by continuity, encourages a corresponding signature of anomalous convergence (Fig. 3c, red shading; Fig. 3d, blue shading) and thereby descending motion (Fig. 3b, red shading) across the tropical Pacific. These convergent signatures, however, are focused largely in the west, an area of climatological ascent (Fig. 3b, gray contours; Fig. 3c, hatching) and upper-level divergence (Fig. 3c, gray contours). As such, decreased precipitation is also observed in these regions (Fig. 3a, brown contours), as are positive sea level pressures (not shown), hence the in-phase correlation with the eqSOI (Fig. 1d). The dynamics of these Atlantic–Pacific interactions are consistent with those of previous model-based studies (Rodríguez-Fonseca et al. 2009; Losada et al. 2010; Ding et al. 2012; Kucharski et al. 2015; Li et al. 2015c).

In addition to the direct response discussed above, Atlantic-induced SST anomalies in the Pacific additionally promote a secondary, or indirect, atmospheric response. Anomalous SST conditions act to amplify WC changes (Fig. 3b), further encouraging anomalous wind conditions, and thus reinforcing the La Niña SST pattern through Bjerknes feedback and associated mechanisms (see also Li et al. 2015c). Using observations, however, it is difficult to separate these direct and indirect atmospheric responses, the combination of which is represented in Fig. 3. Sections 3d and 3e will consequently address this issue using idealized model simulations.

It is clear, however, that the WC represents an atmospheric bridge between the Atlantic and Pacific, providing the mechanism through which the impacts of ATL3 variability may be transferred to the Pacific in order to trigger ENSO-like teleconnections (be it from the direct or indirect WC responses outlined above). Of particular dynamical interest is the anomalous occurrence of upper-level convergence across the central/western Pacific (Figs. 3c,d, shading), a region typified by climatological divergence due to the west Pacific warm pool (Fig. 3c, contours). These changes in the WC create anomalous vorticity forcing that allows for Rossby wave excitation, consistent with the well-established ENSO teleconnection dynamics (Karoly 1989; Trenberth et al. 1998). Despite large-scale convergence over the Pacific, Rossby wave source (RWS; Sardeshmukh and Hoskins 1988) anomalies, which define vorticity forcing associated with upper-level divergence and low-level convergence, are small within the equatorial latitudes due to the dependence on absolute vorticity (Fig. 3d, contours). Driven by corresponding changes in the local Hadley cells, effective sources may thus be nonlocal, and focused in the subtropics where westerly flow aids in wave train production (Rasmusson and Mo 1993; Trenberth et al. 1998). Specifically, the pronounced negative RWS anomaly located over the central subtropical Pacific may be pivotal, but further work is required to discern the dominant sources and their role in promoting Rossby waves. Nevertheless, it can be suggested that a component of the ATL3 teleconnection outlined in Fig. 2a arises from Atlantic–Pacific interactions, specifically the anomalous WC-driven convergence signatures, and the subsequent excitation of stationary Rossby waves from the Pacific, expressed as ENSO-like anomalies. Henceforth, these shall be discussed as the WC-driven components of ATL3 teleconnections (Fig. 2e).

Concurrently, physical processes act to trigger the Atlantic Rossby wave train, that is the alternating pattern of positive and negative Z_{200} anomalies that propagate eastward from the subtropical Atlantic (Fig. 2c). Increased equatorial SST (Fig. 3a, shading) and the associated interaction with the ITCZ drive anomalous vertical motion (Fig. 3b, shading), deep convection (Fig. 3a, contours), and thus upper-level divergence (Fig. 3d, shading) over the equatorial Atlantic. Given the climatological characteristics of the meridional circulation during austral winter, namely the dominant SH HC (Fig. 3e, black vectors; quantified using vertical velocity and the meridional component of the divergent winds averaged over the Atlantic), corresponding divergent wind anomalies are deflected south (Fig. 3d, vectors), intensifying the local Atlantic HC (Fig. 3e, red vectors). By continuity, anomalous upper-level convergence is observed at the descending branch, centered largely at 30°S, 320°E (Figs. 3d and 3e, shading). This region consequently becomes a strong RWS (Fig. 3d, contours), allowing for wave train excitation well removed from the heating source. The observational dynamical processes presented here reaffirm the mechanisms outlined in the modeling studies of Simpkins et al. (2014) and Li et al. (2015a). In addition to the WC-driven component explained above, ATL3 teleconnections are simultaneously composed of an Atlantic wave train triggered by an intensification of the local Hadley circulation. We subsequently refer to the latter as the HC-driven components of ATL3 teleconnections (Fig. 2c).

Using observations and reanalyses, the dynamical connections between ATL3 SST variability and wintertime teleconnections have been identified, and are suggested to be the product of two interrelated processes that produce wave trains to Antarctica. In both instances, these occur as the result of anomalous vorticity forcing that allows for Rossby wave excitation. The difference, however, is the process through which the waves are forced; in one case through perturbations to

the tropical zonal overturning circulation, and in the other through perturbations to the meridional overturning circulation. In the case of the former, Atlantic SST forcing modifies the (zonal) Walker circulation in two ways: 1) directly as a Gill-type response to tropical convection, and 2) indirectly through an SST-induced WC amplification (Li et al. 2015c). Such WC perturbations promote anomalous upper-level convergence across the central/western Pacific, triggering a Rossby wave that is expressed as ENSO-like geopotential height anomalies; these are referred to as WC-driven features. Increased SST in the tropical Atlantic simultaneously intensifies the local (meridional) Atlantic Hadley circulation through a stronger ITCZ. Upper-level convergence is consequently enhanced at the descending branch of the Hadley cell, creating an RWS from which a wave train emerges. The Rossby wave train manifests as a pattern of positive and negative height anomalies across the SH extratropics. Observed Atlantic teleconnections seem to reflect the superimposed impact of these two (WC- and HC-driven) mechanisms, which in many instances share overlapping centers of action to amplify local circulation features.

d. Model ATL3 teleconnections

To verify the dynamics of ATL3 teleconnections (i.e., the proposed two-mechanism WC- and HC-driven components described above), we additionally perform experiments with an AGCM (CAM5). Full details are outlined in section 2, but briefly we force CAM5 with SST anomalies that represent the monthly spatial pattern of positive (ATL3W) and negative (ATL3C) ATL3 events (Fig. A1). Given the apparent importance of Pacific SST anomalies in amplifying WC changes (i.e., the indirect response), we initially examine simulations forced with the full SST pattern in both the Atlantic and Pacific. Subsequent experiments, as discussed in section 3e, isolate the role of individual basins to verify that resulting teleconnections are not solely Pacific-driven. The impacts of ATL3W/ATL3C are determined by subtracting their results from a control (CTL) simulation forced with climatological SST. Figure 4 displays the wintertime (JJA) Z_{200} anomalies associated with (a) ATL3W, (b) ATL3C, and (c) the difference between the two; as in previous figures, solid red (dashed blue) contours denote positive (negative) anomalies. While we analyze the full 80 years, we note that subsequent results are stable after ~50 model years, demonstrating robustness.

In comparing the high-latitude teleconnections between ATL3W and ATL3C (Figs. 4a and 4b, respectively), the responses can be considered fairly linear. The location and magnitude of Z_{200} anomalies are largely consistent, specifically in relation to the circulation structures in the Atlantic and Pacific. In fact the spatial correlation is −0.59. Given this roughly linear response, consistent with the findings of Li et al. (2015a), we focus subsequent analyses on the difference between the two experiments (i.e., ATL3W − ATL3C). Doing so also provides a more equal comparison to observational regressions, which, by definition, factor in the linearity associated with positive and negative events. We note, however, that the magnitude of modeled anomalies will resultantly be double those of observations.

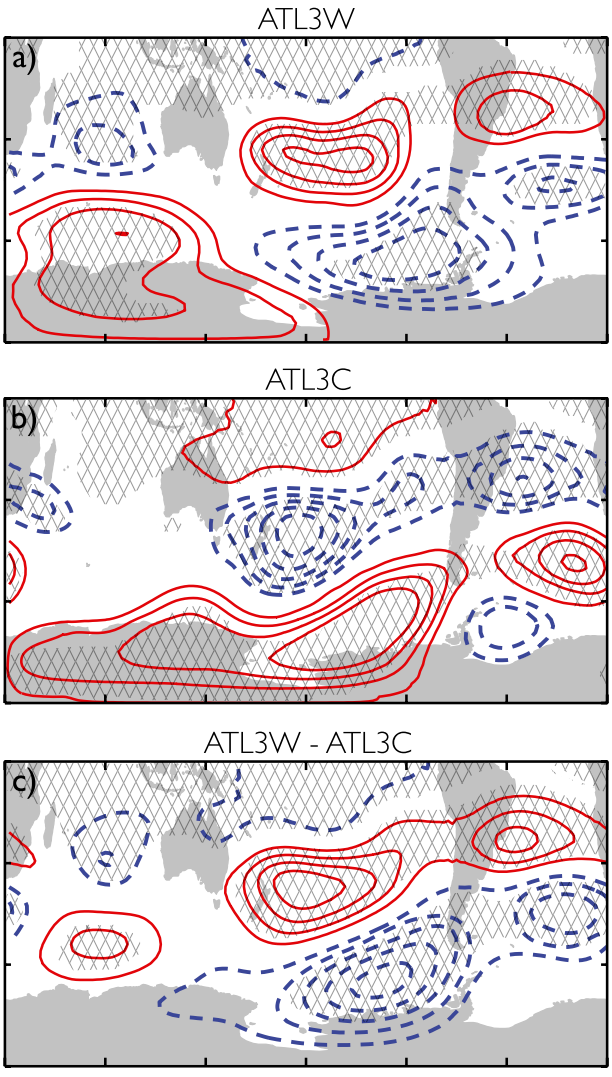

FIG. 4. JJA Z_{200} anomalies from the (a) ATL3W and (b) ATL3C AGCM experiments (see section 2). (c) The difference between ATL3W and ATL3C. Solid red (dashed blue) contours represent positive (negative) anomalies, and are drawn at 5-m intervals for (a) and (b), and 10-m intervals for (c). Hatching in (a) and (b) highlights where ATL3W and ATL3C are significantly different from the CTL, respectively, and in (c) where ATL3W and ATL3C are significantly different from each other.

Figure 4c reveals clear high-latitude teleconnections associated with ATL3 SST variability. Notable large-scale features are found to be similar to observations (cf. Figs. 2a and 4c), both in regard to WC (Pacific-centered) and HC- (Atlantic-centered) driven components, with a spatial correlation of 0.54. However, several differences are apparent. In general the amplitude of modeled teleconnections is greater than that of observations, especially in regard to the Pacific Z_{200} anomalies. In addition, the exact location of structures varies somewhat, as most clearly demonstrated by the more easterly location of negative Z_{200} anomalies in the high-latitude South Pacific. Both these factors point to the dominance of WC-driven components, that is, stronger ENSO-like signals (see Fig. 2e) over the Atlantic wave train (Fig. 2c). Nevertheless, the model does a very reasonable job at capturing the features of interest, demonstrating that SSTs are driving the observed teleconnections, and that the model can be used to validate the atmospheric dynamics. Recall that ATL3 and SAM indices are uncorrelated during JJA.

To evaluate whether the model-derived WC and HC-driven mechanisms are similar to observations, Fig. 5 displays the difference in tropical variables between ATL3W and ATL3C. In comparing Figs. 3 and 5, it is apparent that the model captures the large-scale tropical changes that drive high-latitude teleconnections. A marked modification to the WC is prevalent (Figs. 5b,c), with changes that are ~25% stronger than the observational counterparts, indicative of increased model sensitivity to Pacific SST anomalies. It is for this reason that WC-driven components may dominate the signals seen in Fig. 4c. In addition, the regions of peak convergence (Figs. 5c,d), as well as climatological ascending motion (Fig. 5c, hatching), have moved toward the central Pacific. Consistent with the observational analyses of Ciasto et al. (2015), such shifts may explain the more eastward location of South Pacific Z_{200} anomalies.

In contrast to the WC-driven components described above, the HC-driven counterparts are typically underestimated by the model. While precipitation (Fig. 5a, contours), vertical velocity (Fig. 5b, shading) and divergence (Fig. 5d, shading) anomalies are largely similar to observations, divergent wind anomalies (Fig. 5d, vectors) are found to flow from a more northerly location (cf. Figs. 3d and 5d), suggestive of a northern bias in the position of the Atlantic ITCZ. Using precipitation as a proxy from the CTL simulation, Fig. 6 quantifies this bias at ~2°latitude in JJA (see also Siongco et al. 2015). Evaluating the climatological HC in the Atlantic reveals a similar shift (Fig. 5e, black vectors) but further illustrates the absence of a dominant SH cell. Given the location of SST anomalies in the equatorial SH (Fig. 5a, shading), interactions with the ITCZ, as well as subsequent perturbations to the Atlantic HC, will therefore be lessened (Fig. 5e, red vectors). Nevertheless, enhanced upper-level convergence is apparent at the descending branch at ~20°–30°S (Fig. 5d, blue shading; Fig. 5e, shading), allowing the establishment of a RWS (Fig. 5d, contours), although this too exhibits a northern bias compared to observations (cf. Figs. 3d and 5d).

Model simulations using CAM5 thus provide support for the two-mechanism teleconnection dynamics hypothesized from observational analyses. In response to ATL3 SST forcing and the associated Pacific SST anomalies, a pronounced perturbation to the WC is simulated, which, given the nature of the simulations, represents both the direct and indirect responses. An eastward bias in the region of maximum convergence is highlighted, as is the increased amplitude of WC changes; these differences account for the contrasts in teleconnection characteristics to observations, specifically the dominance of WC-driven components. At the same time the modeled HC undergoes intensification, but the simulated overturning increase is weaker than seen in observations because of a northern bias in ITCZ location and the resulting weakened interaction with SST anomalies. Despite these subtle differences, model simulations provide supporting evidence that ATL3 teleconnections are the product of superimposed WC- and HC-driven components.

e. *Isolating the role of Atlantic and Pacific SST anomalies*

While the ATL3 simulations reveal similar tropical characteristics to observations, and seemingly verify the proposed two-mechanism process, it is important to validate that any subsequent teleconnections are not simply the result of including Pacific SST anomalies (Fig. 5a, shading; Fig. A1), which are well known to impact the SH high latitudes. In addition, we also aim to obtain further information regarding the dominant processes driving such teleconnections. Simulations were therefore repeated wherein SST signals were constrained to the Atlantic only ($ATL3W_{AO}$ and $ATL3C_{AO}$) and the Pacific only ($ATL3W_{PO}$ and $ATL3C_{PO}$), removing ATL3-related SST anomalies in the Pacific and Atlantic, respectively; note that SST forcing of the former is qualitatively similar to that in which the ENSO signature has been linearly removed (Fig. A1, contours). As in previous figures, we focus on the ensemble difference between warm and cold simulations.

As depicted in Fig. 7, the high-latitude atmospheric signatures associated with the Atlantic-only experiments bear strong resemblance to the ATL3W/ATL3C counterparts (cf. Figs. 7c and 7h). Spatial correlations between these two experiments are 0.70, verifying that total ATL3 teleconnections may primarily be linked to Atlantic SST variability. Indeed, while the Pacific only

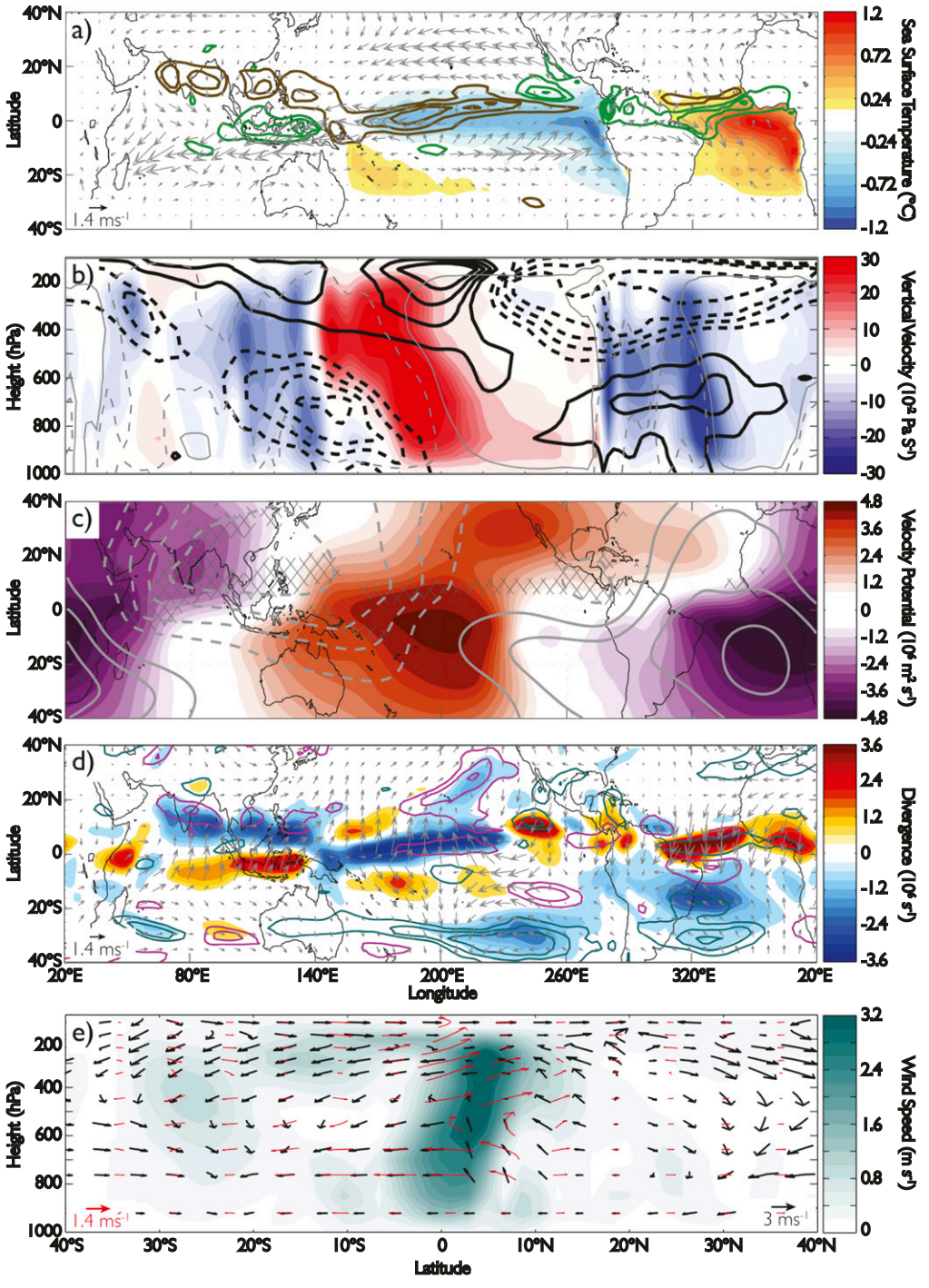

FIG. 5. Wintertime (JJA) difference between ATL3W and ATL3C AGCM experiments for (a) SST (shading), 925-hPa winds (vectors), and precipitation (contours); (b) vertical velocity (shading) and zonal wind (contours) averaged over 5°N/S; (c) 200-hPa velocity potential (shading); (d) 200-hPa divergence (shading), divergent wind (vectors), and Rossby wave source (contours), and (e) Atlantic Hadley circulation wind speed (shading) and winds (red vectors). In (a), green (brown) contours denote increased (decreased) precipitation, drawn at 1 mm day^{-1} intervals. In (b) solid (dashed) contours denote positive/eastward (negative/westward) winds, drawn at 1 m s^{-1} intervals. Gray contours mark the climatological vertical velocity averaged over 5°N/S, with solid (dashed) contours indicating the boundaries of descending (ascending) cells at 0.01 m s^{-1}. In (c), contours represent the climatological mean velocity potential from the CTL simulation, with solid (dashed) contours denoting negative-convergent (positive-divergent) values, drawn at 4×10^6 m^2 s^{-1}, and hatching where climatological ascending motion is observed. In (d), pink (turquoise) contours denote positive (negative) Rossby wave source anomalies, drawn at 0.5×10^6 s^{-2} intervals. In (e), black vectors denote the climatological Atlantic Hadley circulation computed from the control simulation.

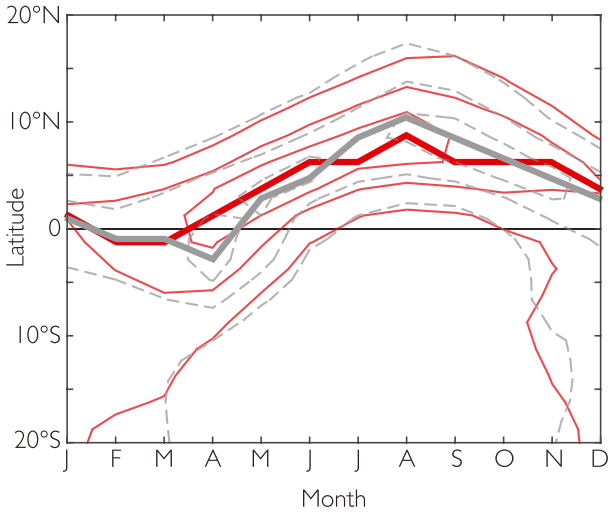

FIG. 6. Monthly climatological mean precipitation averaged over 300°–20°E for observations (red) and the CTL ACGM experiment (gray). Contours are drawn at 2 mm day^{-1} intervals, with the zero contour omitted. Thick lines denote the latitude of the monthly maximum as a representation of the ITCZ.

simulations exhibit similar spatial characteristics (e.g., positive (negative) Z_{200} structures over the subtropical (high latitude) South Pacific), these are of comparatively minor amplitude, suggesting that Pacific SST anomalies related to Atlantic variability play a subsidiary, yet modulating, role through amplifying Atlantic-driven features. The Atlantic- and Pacific-only simulations therefore combine almost linearly to reproduce the total ATL3 teleconnection (cf. Figs. 7g and 7h), supporting earlier observational results in which Atlantic and Pacific variability was isolated (Fig. 2). In fact, these model results compare reasonably well to their observational counterparts: $ATL3_{AO}$ (Fig. 7c) and $ATL3_{eqSOIRemoved}$ (Fig. 2c), as well as $ATL3_{PO}$ (Fig. 7f) and $eqSOI_{ATL3Removed}$ (Fig. 2e), share many dominant features. In $ATL3_{AO}$, however, the well-separated Z_{200} features seen in observations are combined to produce a more zonally elongated teleconnection. In addition, ATL_{PO} Z_{200} features are weaker and shifted compared to observations, likely the result of contrasting nature of the associated forcing (e.g., atmospheric eqSOI versus SST-driven numerical simulations). These additional simulations thus reveal that the direct impact of Atlantic SST dominates, but that synchronous ATL3-related SST variability in the Pacific acts to enhance, or feed back on, the resulting teleconnection.

Recall from section 3c that Atlantic SST anomalies drive Pacific WC variability in two ways: 1) directly as a Gill-type response and 2) indirectly through SST-induced amplification (see also Li et al. 2015c). The $ATL3_{AO}$ and $ATL3_{PO}$ experiments enable further clarification as to the relative importance of these two processes. While fully or partially coupled simulations are required for full diagnosis, these experiments nevertheless allow for increased dynamical interpretation, at least in an idealized sense. By removing the Pacific SST signatures, for example, the Atlantic-only simulations largely represent the direct WC response by excluding Pacific-driven SST feedbacks to the atmosphere. In doing so, atmospheric changes significantly weaken or disappear over the tropical Pacific (Figs. 8a–d). These differences are most evident with regard to the WC, in which total perturbations are dramatically minimized (cf. Figs. 5b and 8b), indicating that this direct Gill-type WC response has little impact on the resulting teleconnections (Figs. 7a–c). The reduced Atlantic–Pacific SST gradient may similarly play a role in minimizing WC perturbations (Wang 2006). Instead, the $ATL3_{AO}$ simulations are dominated by significant changes to the Atlantic HC, with magnitudes that closely resemble those of the full ATL3 experiments (cf. Figs. 5e and 8e). Accordingly, the high-latitude $ATL3_{AO}$ signatures (Figs. 7a–c)—and by virtue of their resemblance, the ATL3 teleconnections—can primarily be attributed to the HC mechanism. Pivotally, these additional simulations reveal that tropical Atlantic SST variability is able to teleconnect to the SH extratropics in the absence of Pacific SST anomalies.

The $ATL3_{PO}$ simulations, however, reveal that Pacific SST anomalies play an important, yet secondary, role in forcing the total ATL3 teleconnection (Fig. 7). These experiments can be considered to represent the indirect WC response, that is, WC amplification associated with SST-induced feedbacks. Figures 8f–i reveal a considerably perturbed WC, with changes that account for a large proportion of those observed in the ATL3 experiments (cf. Figs. 5b and 8g). Total WC changes are thus controlled primarily by the indirect response, with impacts for the resulting teleconnections. Specifically, upper-level convergent signatures (Figs. 8h,i) initiate a Rossby wave (Fig. 7f), the impacts of which amplify the HC-driven Z_{200} features related directly to Atlantic SST (Fig. 7c). By contrast, the Atlantic HC responses are small in the Pacific only simulations (Fig. 8j), suggestive of a limited back influence of Pacific SST anomalies on the Atlantic.

Through isolating the impacts of ATL3-related SST variability in the Atlantic and Pacific, it is found that both basins combine linearly to produce the total teleconnection to the SH extratropics (Fig. 7). Shown schematically in Fig. 9a, Atlantic SSTs are found to dominate, driving marked changes to the local HC that allow for subsequent Rossby wave excitation (Figs. 8a–e and 9, purple features): the so-called HC-driven components. The corresponding Gill-type response to Atlantic convection has minor bearing on the WC, and thus

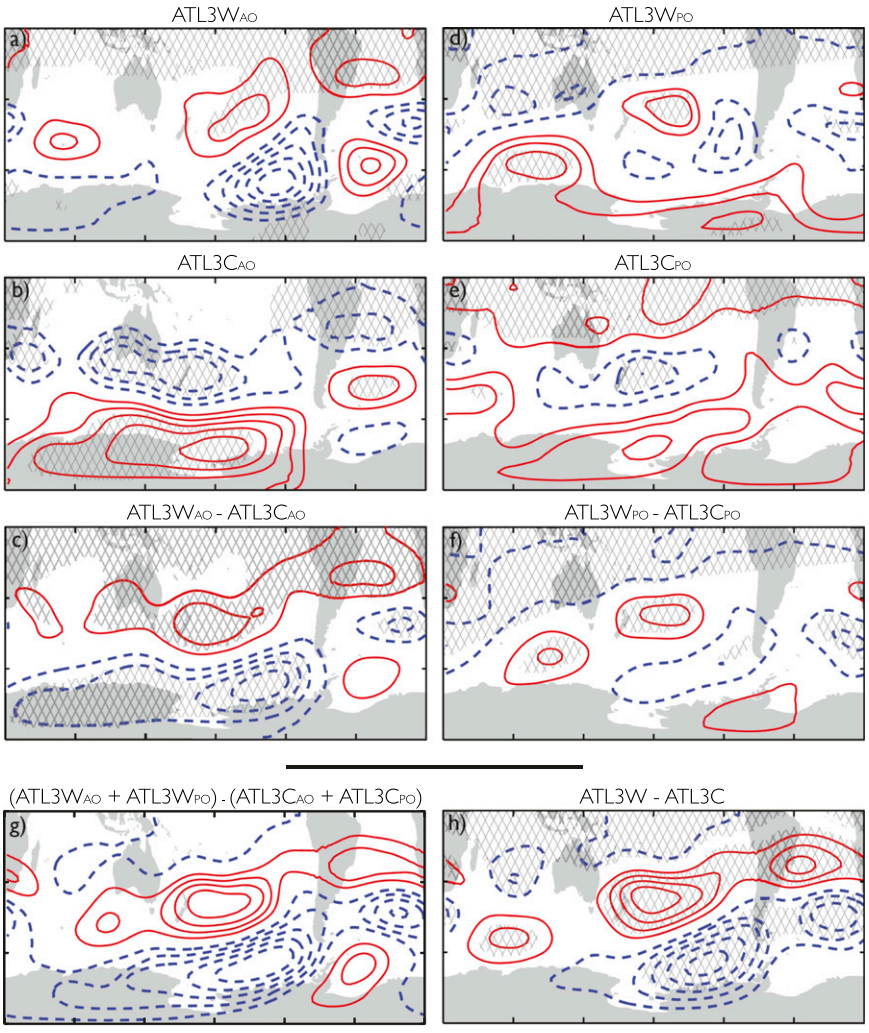

FIG. 7. As in Fig. 4, but for the (left) $ATL3_{AO}$ and (right) $ATL3_{PO}$ AGCM experiments in which SST anomalies are constrained to the Atlantic and Pacific only, respectively. (g) The sum of Atlantic-only and Pacific-only differences, to compare to (h) the total ATL3 difference.

little effect on high-latitude teleconnections (Fig. 8b). However, through WES feedbacks and associated mechanisms, these WC changes drive a La Niña–like SST pattern, with subsequent impacts. Such Pacific SST anomalies act to amplify the local WC response (the indirect effect; Figs. 8f–i) and, in doing so, initiate an ENSO-like teleconnection to the SH high latitudes (Fig. 7f). These WC-driven features are shown schematically in Fig. 9b (gray features). The combination of these two processes—the primary Atlantic-induced HC changes (Fig. 9a) and the secondary Pacific-induced WC changes (Fig. 9b)—results in the total teleconnection we observe (Fig. 7h).

4. Summary and conclusions

A few recent studies have identified links between tropical Atlantic SST variability and the circulation in the extratropical SH (Li et al. 2014, 2015a,b; Simpkins et al. 2014). Here, using observational datasets and CAM5 AGCM experiments, we further document these Atlantic teleconnections. Particular emphasis was given to diagnosing the possible mediating role of Pacific processes, which to date remain largely unexplored. The key conclusions from this study include the following:

1) Atlantic teleconnections to the SH extratropics represent a two-mechanism process, wherein the superposition of Atlantic and Pacific-driven anomalies constitutes the overall high-latitude response.

   In austral winter, synchronous variability is observed between tropical Atlantic SST and the Pacific atmosphere (Fig. 1). As a result, the corresponding high-latitude teleconnections bear marked similarities (Figs. 2a and 2b), indicating that Atlantic signatures

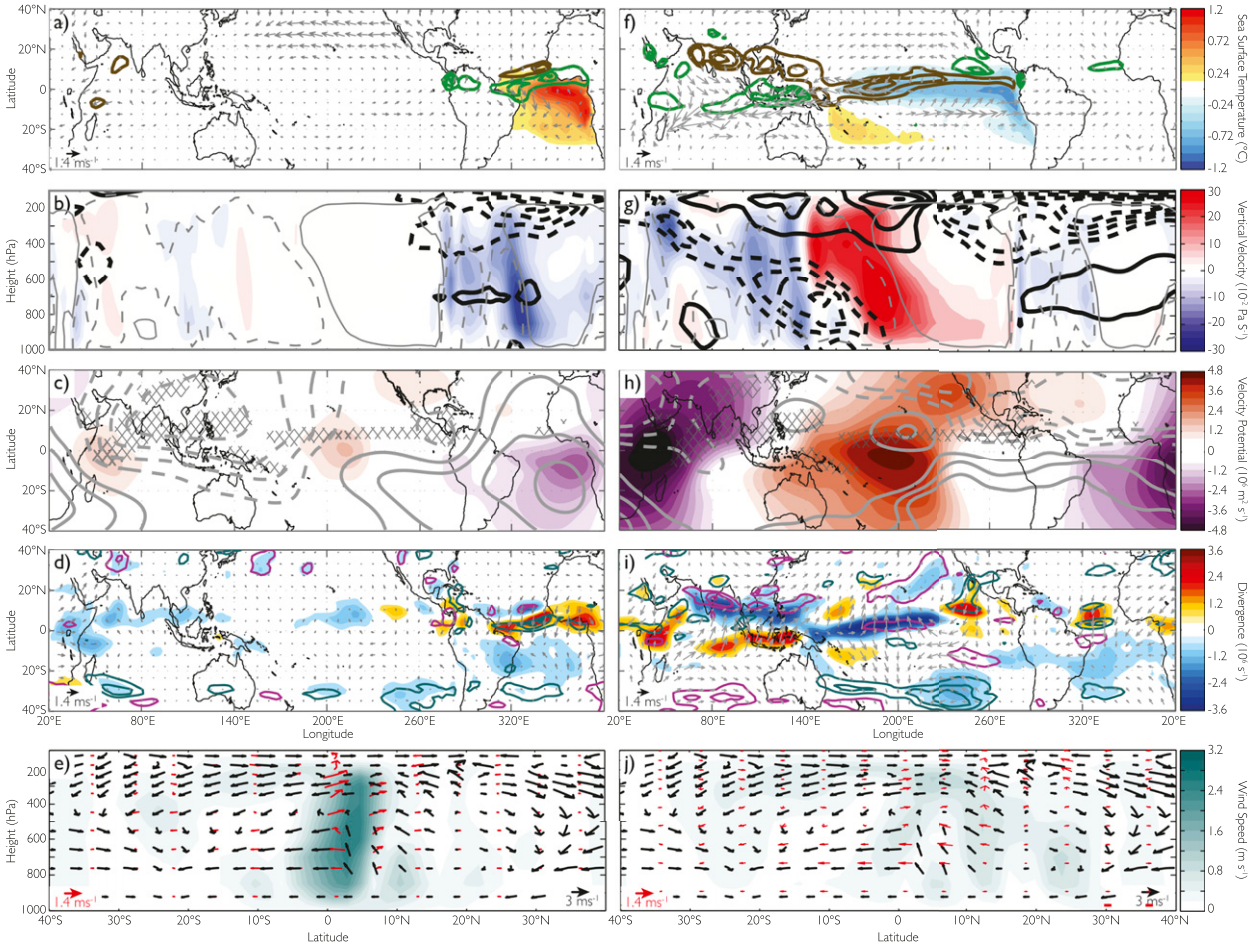

FIG. 8. As in Fig. 5, but for the (left) $ATL3_{AO}$ and (right) $ATL3_{PO}$ AGCM simulations.

may be impacted by Pacific processes. Indeed, when isolating variability in each basin (i.e., by linearly removing signals from the opposing index), it is revealed that Atlantic teleconnections are composed of two individual, yet interrelated, patterns: 1) a Rossby wave train extending from the central Pacific, expressed as ENSO-like anomalies, and driven through Atlantic–Pacific interactions (Fig. 2e), and 2) wavelike anomalies extending east across the extratropical Atlantic in the SH (Fig. 2c). The sum of these two signatures gives the observed ATL3 teleconnection (Fig. 2f), and as both share many overlapping features, distinct regions of heightened pressure anomalies are observed, such as over the ASL. Given a correlation of 0.64, it can be suggested that ~40% of ATL3 teleconnection components may be Pacific-related. While Atlantic SST is shown to impact the extratropical SH atmosphere, the variability explained by these teleconnections is fairly small (maximum ~15 m in the high-latitude South Pacific), suggesting that other processes, or a combination thereof, drive most of the variability in this region.

2) Changes to the Walker and Hadley circulations promote the excitation of atmospheric Rossby waves from the Pacific and Atlantic, respectively, driving the two components of observed Atlantic teleconnections.

Both observations and AGCM experiments were used to diagnose the atmospheric dynamics behind the two simultaneous components of Atlantic teleconnections. As summarized schematically in Fig. 9, increased tropical Atlantic SST promotes marked changes to the zonal (Walker) and meridional (Hadley) circulations (Figs. 3 and 5). In both instances, Rossby wave propagation underpins how the tropics influence the extratropics, wherein anomalous upper-level vorticity, nonlocal to the heating source, explains the two teleconnection (i.e., WC-driven and HC-driven) components. Specifically, the mechanisms are as follows:

- *HC-driven components:* Increased equatorial Atlantic SST anomalies interact with the ITCZ to promote ascending motion and upper-level

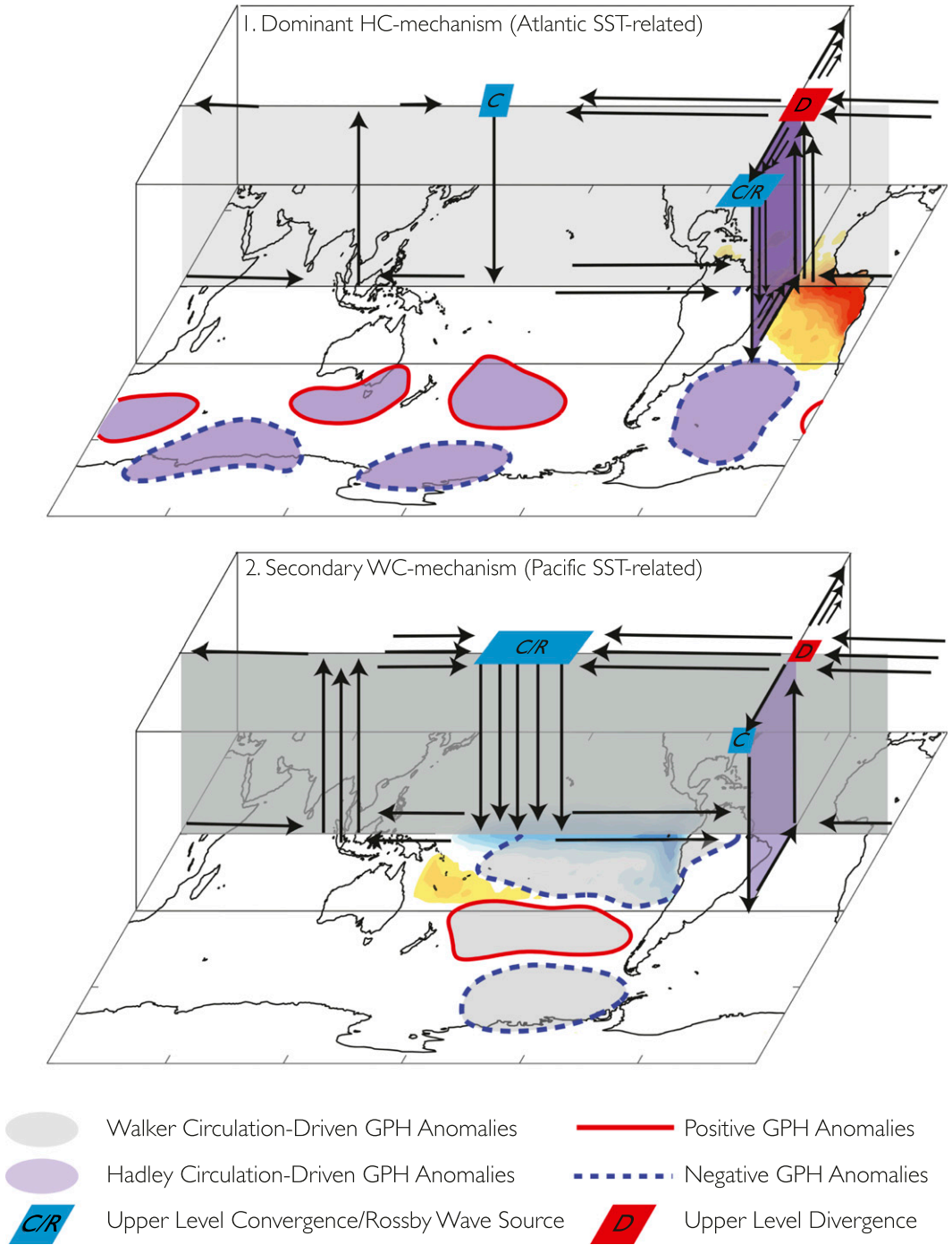

FIG. 9. Schematic summarizing how wintertime ATL3 teleconnections are the product of two interrelated processes: (a) Hadley circulation (HC)-driven height anomalies (purple) associated with Atlantic SST anomalies, and (b) Walker circulation (WC)-driven height anomalies (gray) associated with Pacific SST anomalies driven by Atlantic–Pacific interactions. The sum of these two wave train mechanisms gives the total ATL3 teleconnection.

divergence (Figs. 3b,d,e,Figs. 5b,d,e, and Figs. 8b,d,e). By continuity, upper-level divergent wind anomalies emerge (Figs. 3d,5d,8d) and are deflected south due to dominant wintertime SH Hadley cell, resulting in an intensification of this divergence (Figs. 3e,5e,8e). Enhanced convergence at the descending branch consequently establishes a Rossby wave source, allowing for the excitation of a Rossby

wave train, expressed as an anomalous pattern of alternating positive and negative geopotential heights (Fig. 2c). Simulations in which SST anomalies are constrained to the Atlantic only ($ATL3_{AO}$) reveal that these HC-driven components dominate the total response (Fig. 7). The dynamics of these teleconnections are consistent with those outlined in Simpkins et al. (2014) and Li et al. (2015a) and are illustrated schematically in Fig. 9a.

- *WC-driven components:* The WC provides an atmospheric bridge between the tropical Atlantic and Pacific, and exhibits a pronounced modification in association with ATL3 events (Figs. 3b,c, Figs. 5b,c, Figs. 8g,h). In particular, upper-level convergent signatures are observed over the Pacific (Figs. 3c,d,Figs. 5c,d, and Figs. 8h,i), resulting in anomalous vorticity forcing that triggers a stationary Rossby wave, manifested as ENSO-like geopotential height anomalies (Figs. 2e,7f). These mechanisms are consistent with the well-established ENSO teleconnection dynamics (Karoly 1989; Trenberth et al. 1998). WC changes can primarily be attributed to the indirect effect, that is, a Pacific SST-induced amplification (Fig. 8c; Li et al. 2015c); the direct Gill-type response plays a very minor role (Fig. 8b) and has little bearing on subsequent teleconnections. While the HC-driven components may dominate, synchronous ATL3-related SST variability in the Pacific thus plays a subsidiary, yet important, role, amplifying the high-latitude response to give the observed teleconnection (Fig. 7). These mechanisms are shown schematically in Fig. 9b.

The results presented here build upon previous studies examining Atlantic teleconnections to the SH extratropics (Li et al. 2014, 2015a,b; Simpkins et al. 2014). To a large extent, the dynamical mechanisms we report are consistent with these findings, specifically in regard to the remote initiation of a wave train due to Hadley circulation intensification. However, we build upon these dynamics by reporting an additional component to Atlantic teleconnections: the ENSO-like anomalies associated with a perturbed Walker circulation, and linked to ATL3-related SST anomalies driven by Atlantic–Pacific interactions. Highlighting this additional mechanism may further explain the seasonality of teleconnections discussed by Li et al. (2015a). In particular, the authors relate the lack of summertime associations to the strength and extension of the subtropical jet, the waveguide. While exerting considerable control on the HC-driven components, Atlantic–Pacific interactions may too have some influence. Figure 1c, for example, illustrates weakened ATL3 anomalies in DJF during a period of heightened climatological SST. The corresponding impacts on the WC will therefore be minimal, limiting the possibility of exciting ENSO-like (WC-driven) signals. This ''missing component'' demonstrates that we cannot consider Atlantic and Pacific teleconnections in isolation; the high-latitude signatures are not independent, but rather intrinsically linked through Atlantic–Pacific interactions.

While this study demonstrates the importance of Atlantic–Pacific interactions in influencing interannual climate variability, both in the tropical Pacific (Fig. 1) and in the SH high latitudes, links have also been made with regard to longer-term climatic trends with similar dynamical interpretations. In particular, recent warming in the Atlantic has been linked to a multidecadal strengthening of the Walker circulation, enhancing the Pacific trade winds and driving a trend toward cooler (warmer) eastern (western) Pacific SST, projecting onto the pattern seen in observations (L'Heureux et al. 2013; McGregor et al. 2014; Li et al. 2015c); this eastern Pacific cooling signature has been further attributed as the cause of the ongoing global warming hiatus (England et al. 2014). By promoting changes to Pacific SST, these longer-term Atlantic–Pacific interactions may similarly drive climatic change in the SH extratropics. Ding et al. (2011), Schneider et al. (2012), and Clem and Fogt (2015), for example, relate wintertime and springtime circulation changes over the ASL to teleconnections associated with SST trends in the western/central and subtropical Pacific, regions known to be affected by the Atlantic (England et al. 2014; McGregor et al. 2014; Li et al. 2015c). As such, it may not be that teleconnections from either the Pacific (Ding et al. 2011; Schneider et al. 2012) or Atlantic (Li et al. 2014; Simpkins et al. 2014) are important in explaining high-latitude trends, but rather a combined impact of both.

To date, the community has often regarded high-latitude teleconnections in isolation. This study, however, demonstrates the need to consider Atlantic–Pacific interactions when evaluating climate variability in the SH extratropics. Future work should therefore focus on diagnosing these relationships in further detail, with the hope of providing increased insight into contemporary and future climatic changes in Antarctica.

Acknowledgments. The authors thank three anonymous reviews for their helpful comments, as well as Laura Ciasto and Ashley Payne for useful discussions of results. This work was supported by NSF Grants AGS-1206120 and AGS-1407360. High performance computing was performed at NCAR's CISL.

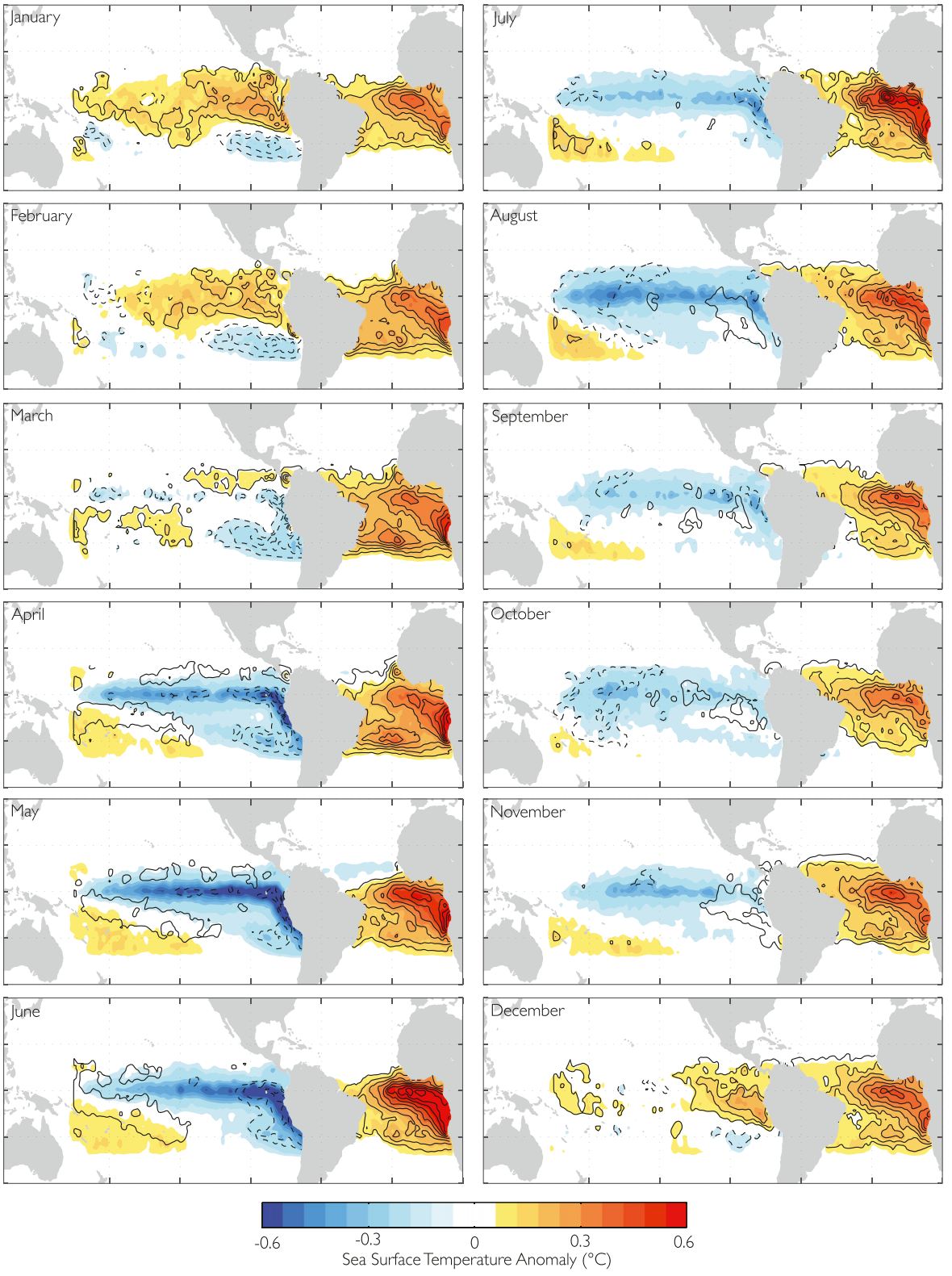

FIG. A1. SST forcing used for the ATL3W AGCM experiments. Figures represent monthly SST anomalies regressed onto the standardized monthly ATL3 index, and constrained between 15°N and 25°S in the Atlantic and Pacific Oceans. Linear damping was applied at these boundaries over a 5° latitude band. ATL3C simulations use the same anomalies but inverted. Contours show regressions in which N3.4 has been linearly removed; solid (dashed) contours denote positive (negative) anomalies, drawn at 0.06°C intervals.

APPENDIX

SST forcing used for the ATL3W AGCM experiments. Figure A1 shows monthly SST anomalies.

REFERENCES

Alexander, M. A., I. Bladé, M. Newman, J. R. Lanzante, N.-C. Lau, and J. D. Scott, 2002: The atmospheric bridge: The influence of ENSO teleconnections on air–sea interaction over the global oceans. *J. Climate*, **15**, 2205–2231, doi:10.1175/1520-0442(2002)015<2205:TABTIO>2.0.CO;2.

Bracegirdle, T. J., 2013: Climatology and recent increase of westerly winds over the Amundsen Sea derived from six reanalyses. *Int. J. Climatol.*, **33**, 843–851, doi:10.1002/joc.3473.

Bretherton, C. S., M. Widmann, V. P. Dymnikov, J. M. Wallace, and I. Bladé, 1999: The effective number of spatial degrees of freedom of a time-varying field. *J. Climate*, **12**, 1990–2009, doi:10.1175/1520-0442(1999)012<1990:TENOSD>2.0.CO;2.

Bromwich, D. H., J. P. Nicolas, A. J. Monaghan, M. A. Lazzara, L. M. Keller, G. A. Weidner, and A. B. Wilson, 2013: Central West Antarctica among the most rapidly warming regions on Earth. *Nat. Geosci.*, **6**, 139–145, doi:10.1038/ngeo1671.

Chang, P., Y. Fang, R. Saravanan, L. Ji, and H. Seidel, 2006: The cause of the fragile relationship between the Pacific El Niño and the Atlantic Niño. *Nature*, **443**, 324–328, doi:10.1038/nature05053.

Ciasto, L. M., G. R. Simpkins, and M. H. England, 2015: Teleconnections between tropical Pacific SST anomalies and extratropical Southern Hemisphere climate. *J. Climate*, **28**, 56–65, doi:10.1175/JCLI-D-14-00438.1.

Clem, K. R., and R. L. Fogt, 2015: South Pacific circulation changes and their connection to the tropics and regional Antarctic warming in austral spring, 1979–2012. *J. Geophys. Res. Atmos.*, **120**, 2773–2792, doi:10.1002/2014JD022940.

Dee, D. P., and Coauthors, 2011: The ERA-Interim reanalysis: Configuration and performance of the data assimilation system. *Quart. J. Roy. Meteor. Soc.*, **137**, 553–597, doi:10.1002/qj.828.

Ding, H., N. S. Keenlyside, and M. Latif, 2012: Impact of the equatorial Atlantic on the El Niño Southern Oscillation. *Climate Dyn.*, **38**, 1965–1972, doi:10.1007/s00382-011-1097-y.

Ding, Q., E. J. Steig, D. S. Battisti, and M. Küttel, 2011: Winter warming in West Antarctica caused by central tropical Pacific warming. *Nat. Geosci.*, **4**, 398–403, doi:10.1038/ngeo1129.

Enfield, D. B., and D. A. Mayer, 1997: Tropical Atlantic sea surface temperature variability and its relation to El Niño–Southern Oscillation. *J. Geophys. Res.*, **102**, 929–945, doi:10.1029/96JC03296.

England, M. H., and Coauthors, 2014: Recent intensification of wind-driven circulation in the Pacific and the ongoing warming hiatus. *Nat. Climate Change*, **4**, 222–227, doi:10.1038/nclimate2106.

Holland, P. R., and R. Kwok, 2012: Wind-driven trends in Antarctic sea-ice drift. *Nat. Geosci.*, **5**, 872–875, doi:10.1038/ngeo1627.

Hosking, J. S., A. Orr, G. J. Marshall, J. Turner, and T. Phillips, 2013: The influence of the Amundsen Bellingshausen Seas low on the climate of West Antarctica and its representation in coupled climate model simulations. *J. Climate*, **26**, 6633–6648, doi:10.1175/JCLI-D-12-00813.1.

Hoskins, B. J., and D. J. Karoly, 1981: The steady linear response of a spherical atmosphere to thermal and orographic forcing. *J. Atmos. Sci.*, **38**, 1179–1196, doi:10.1175/1520-0469(1981)038<1179:TSLROA>2.0.CO;2.

Huang, B., 2004: Remotely forced variability in the tropical Atlantic Ocean. *Climate Dyn.*, **23**, 133–152, doi:10.1007/s00382-004-0443-8.

Jin, D., and B. P. Kirtman, 2009: Why the Southern Hemisphere ENSO responses lead ENSO. *J. Geophys. Res.*, **114**, D23101, doi:10.1029/2009JD012657.

Karoly, D. J., 1989: Southern Hemisphere circulation features associated with El Niño–Southern Oscillation events. *J. Climate*, **2**, 1239–1252, doi:10.1175/1520-0442(1989)002<1239:SHCFAW>2.0.CO;2.

Keenlyside, N. S., and M. Latif, 2007: Understanding equatorial Atlantic interannual variability. *J. Climate*, **20**, 131–142, doi:10.1175/JCLI3992.1.

Kucharski, F., F. S. Syed, A. Burhan, I. Farah, and A. Gohar, 2015: Tropical Atlantic influence on Pacific variability and mean state in the twentieth century in observations and CMIP5. *Climate Dyn.*, **44**, 881–896, doi:10.1007/s00382-014-2228-z.

L'Heureux, M. L., S. Lee, and B. Lyon, 2013: Recent multidecadal strengthening of the Walker circulation across the tropical Pacific. *Nat. Climate Change*, **3**, 571–576, doi:10.1038/nclimate1840.

Li, X., D. M. Holland, E. P. Gerber, and C. Yoo, 2014: Impacts of the north and tropical Atlantic Ocean on the Antarctic Peninsula and sea ice. *Nature*, **505**, 538–542, doi:10.1038/nature12945.

——, E. P. Gerber, D. M. Holland, and C. Yoo, 2015a: A Rossby wave bridge from the tropical Atlantic to West Antarctica. *J. Climate*, **28**, 2256–2273, doi:10.1175/JCLI-D-14-00450.1.

——, D. M. Holland, E. P. Gerber, and C. Yoo, 2015b: Rossby waves mediate impacts of tropical oceans on West Antarctic atmospheric circulation in austral winter. *J. Climate*, **28**, 8151–8164, doi:10.1175/JCLI-D-15-0113.1.

——, S.-P. Xie, S. T. Gille, and C. Yoo, 2015c: Atlantic-induced pan-tropical climate change over the past three decades. *Nat. Climate Change*, **6**, 275–279, doi:10.1038/nclimate2840.

Losada, T., B. Rodríguez-Fonseca, I. Polo, S. Janicot, S. Gervois, F. Chauvin, and P. Ruti, 2010: Tropical response to the Atlantic equatorial mode: AGCM multimodel approach. *Climate Dyn.*, **35**, 45–52, doi:10.1007/s00382-009-0624-6.

Lübbecke, J. F., and M. J. McPhaden, 2012: On the inconsistent relationship between Pacific and Atlantic Niños. *J. Climate*, **25**, 4294–4303, doi:10.1175/JCLI-D-11-00553.1.

Matthewman, N. J., and G. Magnusdottir, 2012: Clarifying ambiguity in intraseasonal Southern Hemisphere climate modes during austral winter. *J. Geophys. Res.*, **117**, D03105, doi:10.1029/2011JD016707.

McGregor, S., A. Timmermann, M. F. Stuecker, M. H. England, M. Merrifield, F.-F. Jin, and Y. Chikamoto, 2014: Recent Walker circulation strengthening and Pacific cooling amplified by Atlantic warming. *Nat. Climate Change*, **4**, 888–892, doi:10.1038/nclimate2330.

Mo, K. C., 2000: Relationships between low-frequency variability in the Southern Hemisphere and sea surface temperature anomalies. *J. Climate*, **13**, 3599–3610, doi:10.1175/1520-0442(2000)013<3599:RBLFVI>2.0.CO;2.

Neale, R. B., and Coauthors, 2012: Description of the NCAR Community Atmosphere Model (CAM5.0). NCAR Tech. Rep. NCAR/TN-486+STR, 268 pp.

Okumura, Y. M., D. Schneider, C. Deser, and R. Wilson, 2012: Decadal–interdecadal climate variability over Antarctica and linkages to the tropics: Analysis of ice core, instrumental, and

tropical proxy data. *J. Climate*, **25**, 7421–7441, doi:10.1175/JCLI-D-12-00050.1.

Parkinson, C. L., and D. J. Cavalieri, 2012: Antarctic sea ice variability and trends, 1979–2010. *Cryosphere*, **6**, 871–880, doi:10.5194/tc-6-871-2012.

Raphael, M. N., and Coauthors, 2016: The Amundsen Sea low: Variability, change, and impact on Antarctic climate. *Bull. Amer. Meteor. Soc.*, **97**, 111–121, doi:10.1175/BAMS-D-14-00018.1.

Rasmusson, E. M., and K. Mo, 1993: Linkages between 200-mb tropical and extratropical circulation anomalies during the 1986–1989 ENSO cycle. *J. Climate*, **6**, 595–616, doi:10.1175/1520-0442(1993)006<0595:LBMTAE>2.0.CO;2.

Rayner, N. A., D. E. Parker, E. B. Horton, C. K. Folland, L. V. Alexander, D. P. Rowell, E. C. Kent, and A. Kaplan, 2003: Global analyses of sea surface temperature, sea ice, and night marine air temperature since the late nineteenth century. *J. Geophys. Res.*, **108**, 4407, doi:10.1029/2002JD002670.

Rodríguez-Fonseca, B., I. Polo, J. García-Serrano, T. Losada, E. Mohino, C. R. Mechoso, and F. Kucharski, 2009: Are Atlantic Niños enhancing Pacific ENSO events in recent decades? *Geophys. Res. Lett.*, **36**, L20705, doi:10.1029/2009GL040048.

Sardeshmukh, P. D., and B. J. Hoskins, 1988: The generation of global rotational flow by steady idealized tropical divergence. *J. Atmos. Sci.*, **45**, 1228–1251, doi:10.1175/1520-0469(1988)045<1228:TGOGRF>2.0.CO;2.

Schneider, D. P., C. Deser, and Y. Okumura, 2012: An assessment and interpretation of the observed warming of West Antarctica in the austral spring. *Climate Dyn.*, **38**, 323–347, doi:10.1007/s00382-010-0985-x.

Simpkins, G. R., L. M. Ciasto, D. W. J. Thompson, and M. H. England, 2012: Seasonal relationships between large-scale climate variability and Antarctic sea ice concentration. *J. Climate*, **25**, 5451–5469, doi:10.1175/JCLI-D-11-00367.1.

——, ——, and M. H. England, 2013: Observed variations in multidecadal Antarctic sea ice trends during 1979–2012. *Geophys. Res. Lett.*, **40**, 3643–3648, doi:10.1002/grl.50715.

——, S. McGregor, A. S. Taschetto, L. M. Ciasto, and M. H. England, 2014: Tropical connections to climatic change in the extratropical Southern Hemisphere: The role of Atlantic SST trends. *J. Climate*, **27**, 4923–4936, doi:10.1175/JCLI-D-13-00615.1.

Siongco, A. C., C. Hohenegger, and B. Stevens, 2015: The Atlantic ITCZ bias in CMIP5 models. *Climate Dyn.*, **45**, 1169–1180, doi:10.1007/s00382-014-2366-3.

Sutton, R. T., S. P. Jewson, and D. P. Rowell, 2000: The elements of climate variability in the tropical Atlantic region. *J. Climate*, **13**, 3261–3284, doi:10.1175/1520-0442(2000)013<3261:TEOCVI>2.0.CO;2.

Thompson, D. W. J., and J. M. Wallace, 2000: Annular modes in the extratropical circulation. Part I: Month-to-month variability. *J. Climate*, **13**, 1000–1016, doi:10.1175/1520-0442(2000)013<1000:AMITEC>2.0.CO;2.

Trenberth, K. E., G. W. Branstator, D. Karoly, A. Kumar, N.-C. Lau, and C. Ropelewski, 1998: Progress during TOGA in understanding and modeling global teleconnections associated with tropical sea surface temperatures. *J. Geophys. Res.*, **103**, 14 291–14 324, doi:10.1029/97JC01444.

Turner, J., 2004: The El Niño–southern oscillation and Antarctica. *Int. J. Climatol.*, **24**, 1–31, doi:10.1002/joc.965.

——, and Coauthors, 2005: Antarctic climate change during the last 50 years. *Int. J. Climatol.*, **25**, 279–294, doi:10.1002/joc.1130.

——, and Coauthors, 2009: Non-annular atmospheric circulation change induced by stratospheric ozone depletion and its role in the recent increase of Antarctic sea ice extent. *Geophys. Res. Lett.*, **36**, L08502, doi:10.1029/2009GL037524.

——, T. Phillips, J. S. Hosking, G. J. Marshall, and A. Orr, 2013: The Amundsen Sea low. *Int. J. Climatol.*, **33**, 1818–1829, doi:10.1002/joc.3558.

Vaughan, D. G., and Coauthors, 2003: Recent rapid regional climate warming on the Antarctic Peninsula. *Climatic Change*, **60**, 243–274, doi:10.1023/A:1026021217991.

Wang, C., 2006: An overlooked feature of tropical climate: Inter-Pacific-Atlantic variability. *Geophys. Res. Lett*, **33**, L12702, doi:10.1029/2006GL026324.

Xie, P., and P. A. Arkin, 1997: Global precipitation: A 17-year monthly analysis based on gauge observations, satellite estimates, and numerical model outputs. *Bull. Amer. Meteor. Soc.*, **78**, 2539–2558, doi:10.1175/1520-0477(1997)078<2539:GPAYMA>2.0.CO;2.

Xie, S.-P., and J. A. Carton, 2004: Tropical Atlantic variability: Patterns, mechanisms, and impacts. *Earth's Climate: The Ocean–Atmosphere Interaction*, Geophys. Monogr., Vol. 147, Amer. Geophys. Union, 121–142.

Zebiak, S. E., 1993: Air–sea interaction in the equatorial Atlantic region. *J. Climate*, **6**, 1567–1586, doi:10.1175/1520-0442(1993)006<1567:AIITEA>2.0.CO;2.